Addendum to Full-Tracking Resolution in DIRAC with 2001 Data

B. Adeva, A. Romero, O. Vázquez Doce

IGFAE, University of Santiago de Compostela, Spain

Abstract

The rate of pion pairs leading to a very small value of $Q_{X,Y}$ in the Full-Tracking reconstruction, due to single-hit inefficiency of SFD, has been significantly reduced with respect to the results presented earlier in DIRAC Note 05-15. The new results nearly overcome this problem by improving the cuts which define MSGC tracking efficiency. They are presented here, for the same accurate description of detector efficiency and backgrounds as in the previous report, following identical conception of figures and tables.

1 Introduction

We present here an improved version of the study made in our earlier note [1] concerning the resolution and tracking efficiency of the Full-Tracking reconstruction in DIRAC, using Monte Carlo. The observation of the relatively large enhancement in the reconstructed Coulomb pairs at Q_X and Q_Y close to zero, clearly related to the single-hit inefficiency of SFD, in conjunction with unability of MSGC's to resolve these pairs, made us re-evaluate the tracking in a more quantitative way.

With experimental knowledge of the average single-hit efficiencies of MSGC's (ϵ_M =90.0 %) and SFD's (ϵ_F = 97.3 %) [2], we are able to calculate the probability that, under certain conditions, a wide-angle pion pair looses the experimental information necessary to measure the track separation, due to combined SFD and MSGC inefficiency. We call this probability *two-track inefficiency* r_0. After comparison of the tracking results [1] with this calculation (which will be described in next section), we found out that the two-track inefficiency for Coulomb pairs (and therefore the enhancement at $Q_{X,Y}$ close to zero), was actually higher than it should be, thus indicating sources of track inefficiency that needed to be further investigated.

Let us review here what are the changes introduced in the tracking system after our investigation, with respect to the selection cuts outlined in note [1] (section 2):

- A dropping procedure for hits far-away from the tracks ($> 3\sigma$) has been introduced. Every MSGC hit is removed, the track re-fitted, and distance evaluated. This procedure decreases significantly the distortion by background hits.
- Space windows for multiple scattering at pattern recognition (taken from detector covariance matrix) are enlarged from 2σ to 2.5σ, in order to increase MSGC efficiency at resolving wide-angle pairs.
- The time difference cut between SFD and VH was increased to $5.5ns$ (magnitude), in order to improve SFD efficiency.
- A 2% track probability cut, applied when the other track had only MSGC hits in one projection, was suppressed. It did have some effect in two-track inefficiency.

- In cases where the pair contains only one hit in X, one hit in X' and two hits in SFD-X (likewise in the other projection), MSGC hits are newly searched for in the vicinity of existing ones, that may have escaped pattern recognition or have been dropped earlier. They are then assigned to closest track. This improves the quality of low Q_X and Q_Y spectra.
- IH detector cuts are slightly simplified, so that no double pulse is required in one track when the other has only two hits in one projection. It decreases two-track inefficiency.
- Charge division of common microstrip in double MSGC clusters is done proportional to pulse-height, rather than by 1/2. It slightly improves $Q_{X,Y}$ spectrum.

Attempts were also made to use MSGC pulse-height information in available hits, in order to improve further the spurious contribution to single-track pairs by providing appropriate veto, defined by the absence of double MSGC pulse. The fine granularity of the MSGC's would overcome the limitation originated by the 6 mm slab width of IH detector. However, Landau tails did not allow further improvement.

2 Cross-check of two-track inefficiency

In absence of detector backgrounds, the wide-angle (distance larger than 1.5 mm) two-track inefficiency r_0 , multiplied by the integrated Coulomb pair rate (up to the maximum Q_T values that emerge from the trigger system), gives us the excess number of events that will be erroneously found by the reconstruction at Q_X and Q_Y close to zero, because one track has been lost. The presence of backgrounds can only decrease this event rate artificially, and the exact calculation must of course be made by Monte Carlo. Independently, the utilisation of IH detector will also decrease this rate (this time not artificially) to the real value r_H, after application of suitable pulse-hight cuts on the extrapolated IH slabs of each candidate track, in A and B layers. Let us recall here that each track is required to have at least two hits in each projection (either SFD or MSGC), and that the pair can be vetoed in absence of single pulses in IH (two tracks) or double pulse (single track). Here again, the exact calculation of r_H can be made by Monte Carlo. The ratio $f_H = r_H/r_0$ has been determined to be 0.50 ± 0.03.

In order to cross-check the tracking performance, we have removed detector backgrounds from the simulation, and inhibited the application of IH cuts. In this simple situation, the observed two-track inefficiency can be compared with the following calculation:

$$r_0^{th} = 2\epsilon_F(1-\epsilon_F)\Big(2\epsilon_M^3(1-\epsilon_M) + 2\epsilon_M^2(1-\epsilon_M)^2\Big) + 2\epsilon_F^2\epsilon_M(1-\epsilon_M)^3 + 2\epsilon_F^2\epsilon_M^2(1-\epsilon_M)^2$$

where ϵ_F and ϵ_M are the single-hit efficiencies of SFD and MSGC. After the changes introduced in the previous section, we obtain from the tracking the (measured) value $r_H^{ms} = f_H \cdot r_0^{ms} = 1.71 \pm 0.03$ %, to be compared with the calculated value, in terms of pure Gaussian efficiencies of MSGC and SFD, $r_H^{th} = f_H \cdot r_0^{th} = 1.28$ %. In both cases detector backgrounds were removed. We find there is acceptable agreement between the two, after checking that the discrepancy can be explained by adjustable track requirements (beam impact parameter for MSGC-only track projections and DC matching distance, 55%), Molière tails of multiple scattering at track pattern recognition (30%), and other rare geometrical effects (15%).

Therefore, we consider that the performance of the tracking is close to its expected value. Certainly, the two-track inefficiency r_H^{ms} can still be reduced by less stringent cuts, but then background level would be compromised. Please note that the efficiency values ϵ_F and ϵ_M in the Monte Carlo have been determined from the entire experimental data sample in 2001, and are subject to very little uncertainty. Moreover, we know that single-hit efficiencies do not depend essentially on track separation, except for very small distances (due to the PSC effect) [2].

3 New results

In figures 1 to 14 and tables 1 to 3 we show the results obtained after the improvements described in previous sections. All figures and tables have identical numbers and captions as those in note [1], in order to facilitate the comparison. For the sake of completeness, let us recall from this reference what is the definition of the analysed quantities and the meaning of the lines indicating efficiency and bias effects.

A comparison is made between the input center-of-mass momentum components and the reconstructed output. Input is defined as the Q_i values for GEANT $\pi^+\pi^-$ pairs that emerge from the target foil [1]. These are considered as *true* values for the reconstruction procedure, and we denote them by Q_i^{gen} (generator pairs). As for the index i is concerned , we will discuss here the quantities Q_X, Q_Y , $|Q_X|$, $|Q_Y|$, $Q_T = \sqrt{Q_X^2 + Q_Y^2}$ and $|Q_L|$, as most representative. Only the last four are actually measurable by the experiment, because

[1] technically it is achieved by a GEANT cut at 1.15 cm away from the target foil position.

the charge sign becomes random at small opening angles, due to multiple scattering. Nevertheless we also include the first two, for the sake of illustration of tracking properties. In any case, let us mention that the alignment procedures include the charge conjugation symmetry as a constraint, and that the precise determination of pionium lifetime does not require any measurement of the charge sign.

It is required that the generated event passes the trigger and that the drift chambers produce one positive and one negative track, with standard χ^2 cuts. The ensemble of these pairs (P_0) is considered as the reference normalisation, for overall efficiency studies. Generic distributions of Q_i^{gen} in P_0 will be denoted by G_0 in the following. A subset $P_1 \subset P_0$ is defined by reconstructed pairs. For every matched pair (between downstream and upstream arms) there will be a reconstructed (measured) value Q_i^{rec} and a generator (true) value Q_i^{gen}. In the next section we analyse the difference $|Q_i^{gen}| - |Q_i^{rec}|$ (which we call *resolution*), as well as the correlation between Q_i^{gen} and Q_i^{rec}, for atom pairs and for Coulomb pairs separately. We will be calling, generically, G_1 and R_1 the distributions of Q_i^{gen} and Q_i^{rec}, respectively, for pairs that belong to P_1.

The following results are presented after a cut $Q_T^{gen} < 6$ MeV/c , where the generator value Q_T^{gen} is defined past the target foil.

In figures 1 to 6 reconstructed Q_i distributions (R_1) are shown for pionium pairs and for Coulomb pairs, and they are compared with generator (true) values G_1. The effects of statistical bias and efficiency, on the one hand, and distortion caused by the measurement, on the other hand, can be decoupled by showing the ratios G_1/G_0 and R_1/G_1 separately. Top and bottom parts are allways associated to pionium and Coulomb pairs, respectively. Figure 7 shows correlation between Q_X^{rec} and Q_X^{gen}, whereas figure 8 provides full information about resolution, including tails. Figures 9 and 10 are dedicated to Q_L, which remains unchanged as expected. Figures 11 and 12 show the Q_X spectrum for different categories according to the number of hits per track, for pionium and Coulomb pairs, respectively. Figure 13 also shows the Q_X spectrum, now separated into two categories, according to whether the two tracks share or not the same SFD hit. Finally figure 14 shows the Q_T spectrum compared with the one that would be obtained by using only SFD hits (when available) in the final fit, but entirely following the selection procedure of the full-tracking method. It should be noted that the latter distribution is *not* the one that would be obtained by using SFD detector alone in the tracking.

Tables 1 and 2 provide all relevant information about resolution for atom pairs and Coulomb pairs, respectively, including positive and negative tails separately. Table 3 specifically addresses the integrals of tails of reconstructed Q_T spectrum for atom pairs.

Table 1
Gaussian resolution σ and fraction of events where $|Q_i^{gen}| - |Q_i^{rec}|$ is larger than 2 MeV/c, for atom pairs. Positive and negative tails are given separately.

	σ (MeV/c)	Tail (+) (%)	Tail (-) (%)
$\|Q_X\|$	0.10	0.10	2.42
$\|Q_Y\|$	0.11	0.09	2.45
Q_T	0.12	0.08	4.10
Q_L	0.52	2.66	2.56

Table 2
Gaussian resolution σ and fraction of events where $|Q_i^{gen}| - |Q_i^{rec}|$ is larger than 2 MeV/c, for Coulomb pairs. Positive and negative tails are given separately.

	σ (MeV/c)	Tail (+) (%)	Tail (-) (%)
$\|Q_X\|$	0.10	1.11	1.13
$\|Q_Y\|$	0.11	1.21	1.19
Q_T	0.12	1.15	1.51
Q_L	0.52	2.77	2.66

Table 3
Fraction of atom pairs reconstructed with two different Q_T cuts, the corresponding fraction for the original generator values (after multiple scattering in the target foil), and the difference between the two.

	tail (%)	generator (%)	loss (%)
$Q_T^{rec} > 4$ MeV/c	3.73	1.09	2.65
$Q_T^{rec} > 5$ MeV/c	2.12	0.31	1.80

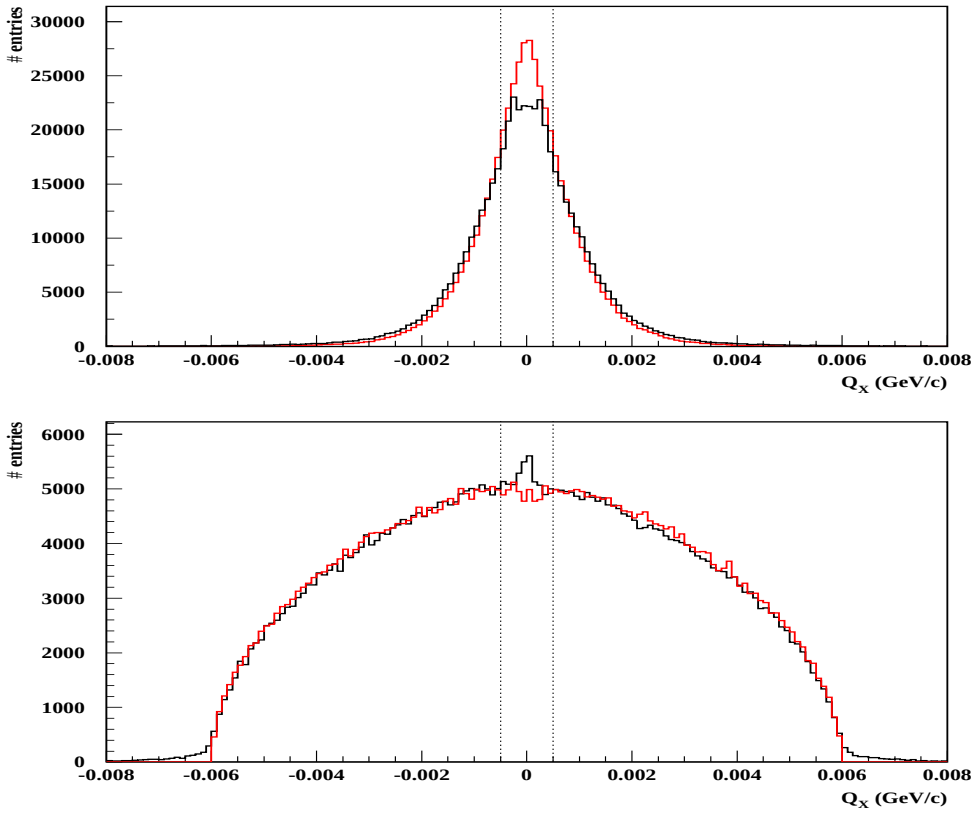

Fig. 1. *Comparison between generated Q_X spectrum G_1 (red), and reconstructed spectrum R_1 (black) for atom pairs (top), and for Coulomb pairs (bottom). See the text for more detail.*

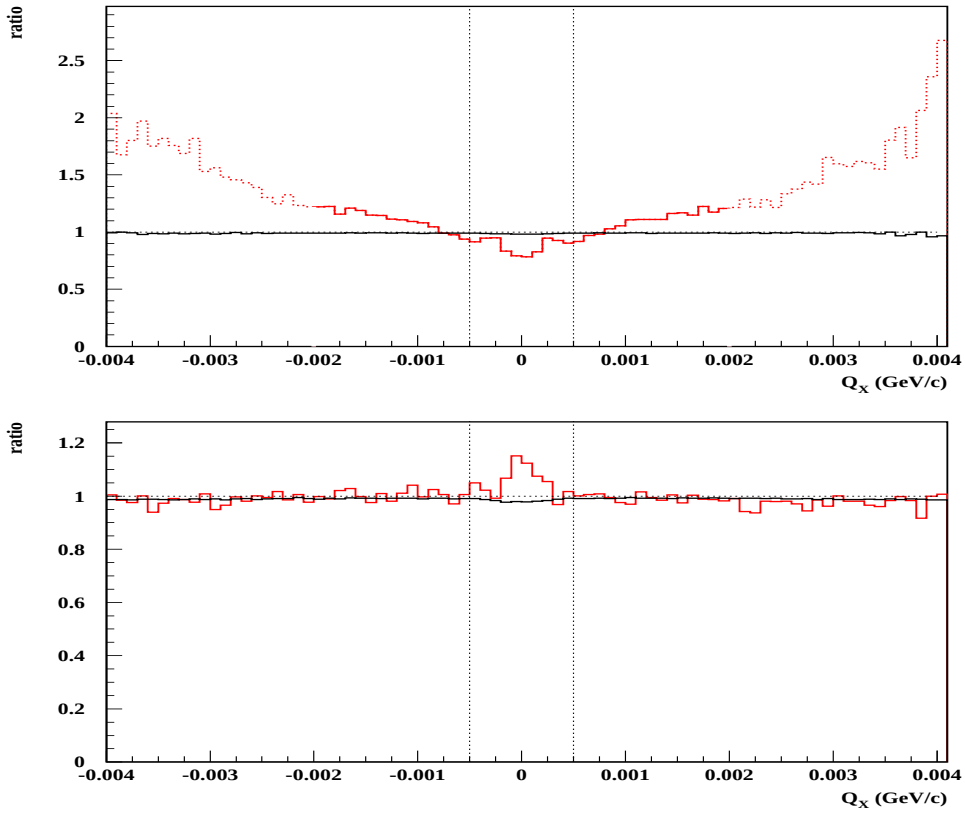

Fig. 2. *Ratios G_1/G_0 (black) and R_1/G_1 (red) for the lines shown in figure 1 for Q_X of atom pairs (top). Corresponding ratios are also given for Coulomb pairs (bottom). See text for more details.*

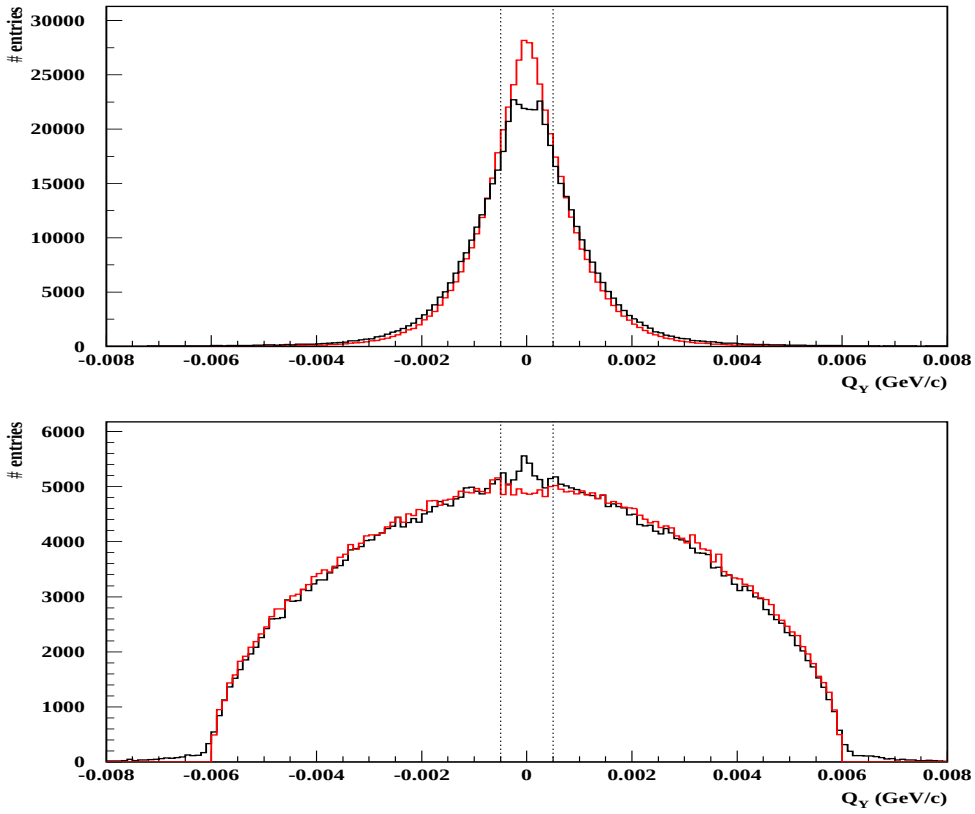

Fig. 3. *Comparison between generated values G_1 (red), and reconstructed (R_1) values (black) of Q_Y for atoms pairs (top), and for Coulomb pairs (bottom). See the text for more detail.*

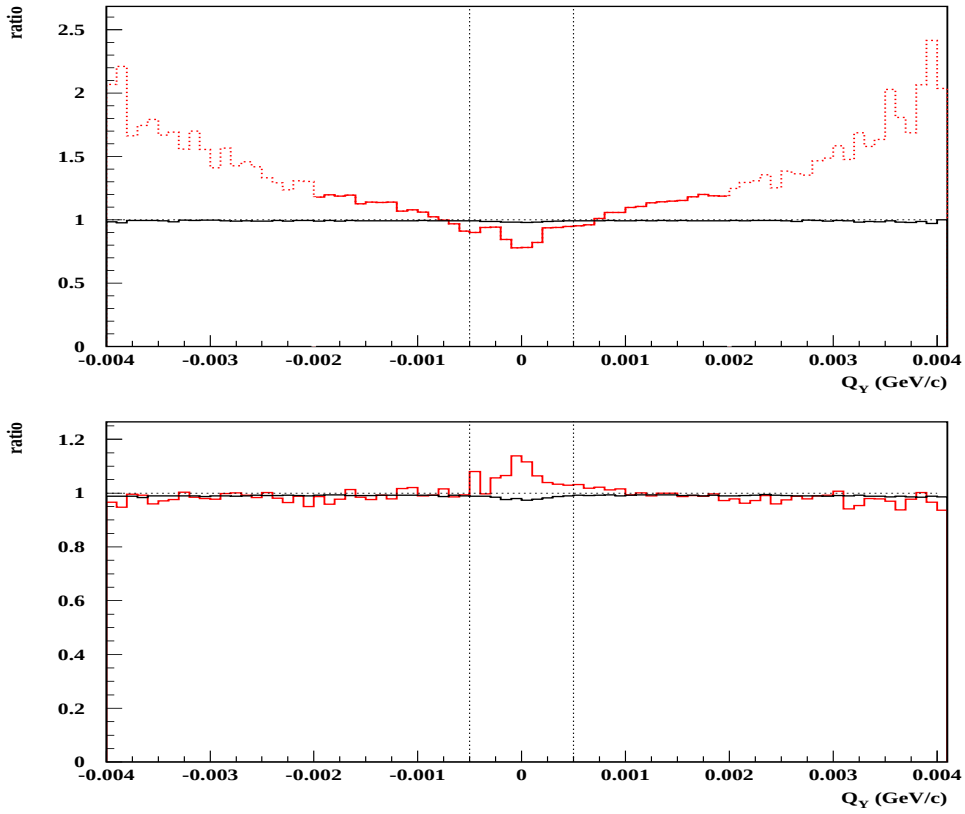

Fig. 4. *Ratios G_1/G_0 (black) and R_1/G_1 (red) for the lines shown in figure 3 for Q_Y of atom pairs (top). Corresponding ratios are also given for Coulomb pairs (bottom). See text for more details.*

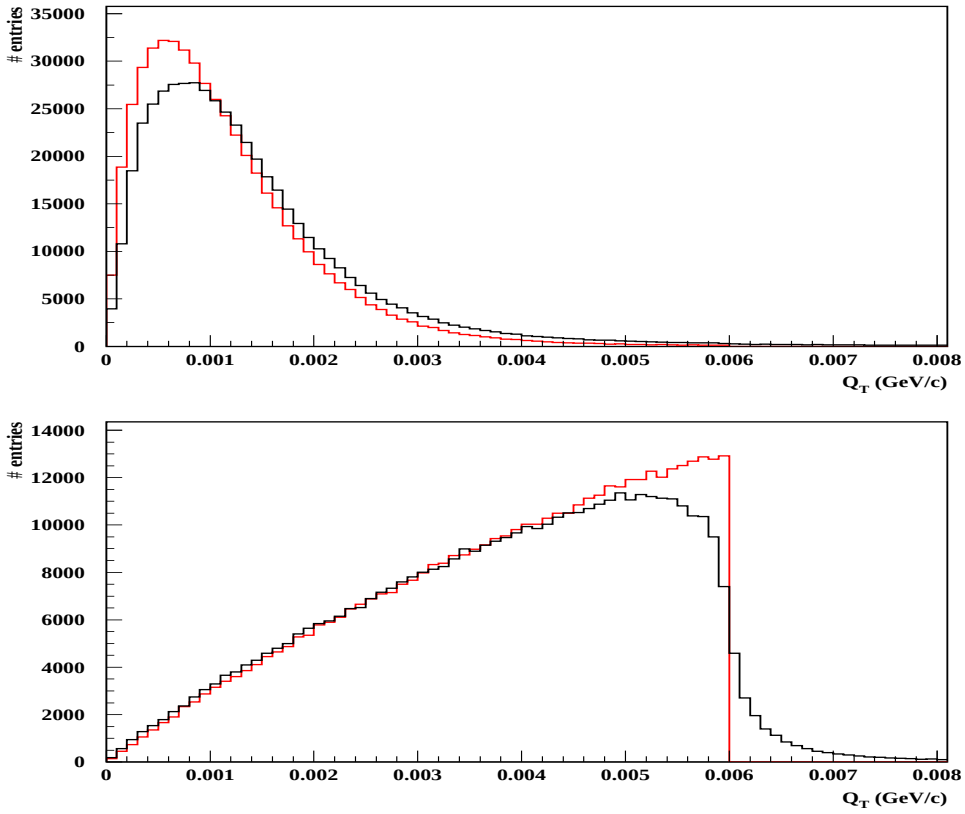

Fig. 5. *Comparison between generated Q_T spectrum G_1 (red), and reconstructed spectrum R_1 (black) for atom pairs (top), and for Coulonb pairs (bottom). See the text for more detail.*

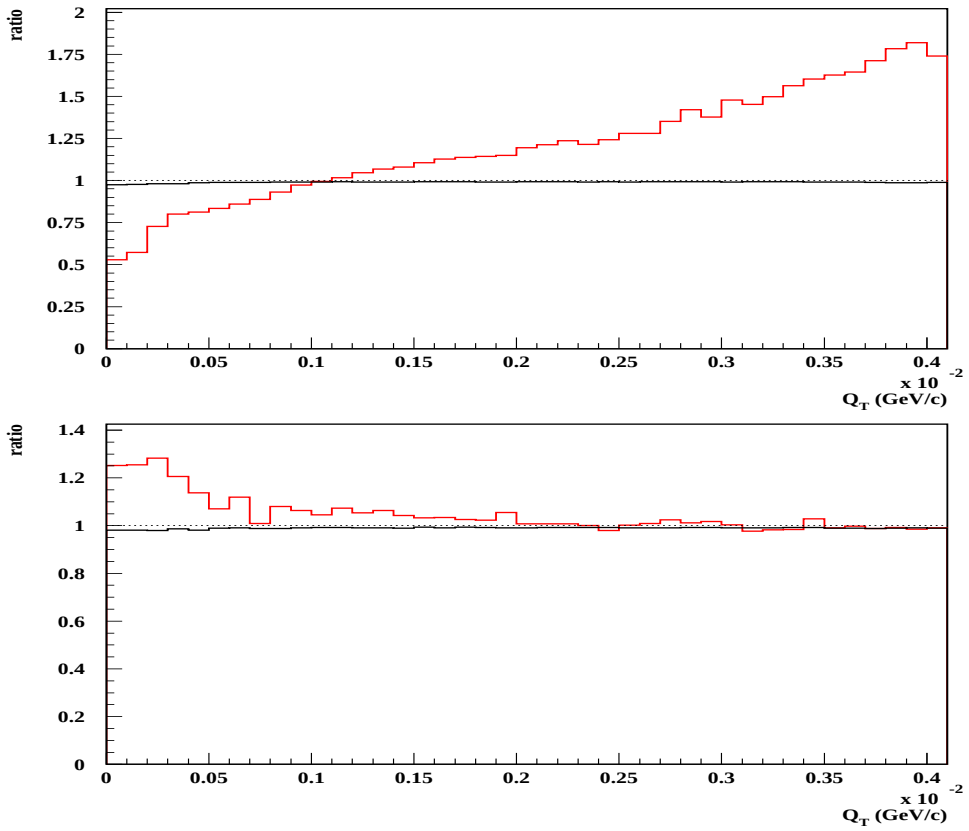

Fig. 6. *Ratios G_1/G_0 (black) and R_1/G_1 (red) for the lines shown in figure 5 for Q_T of atom pairs (top). Corresponding ratios are also given for Coulomb pairs (bottom).*

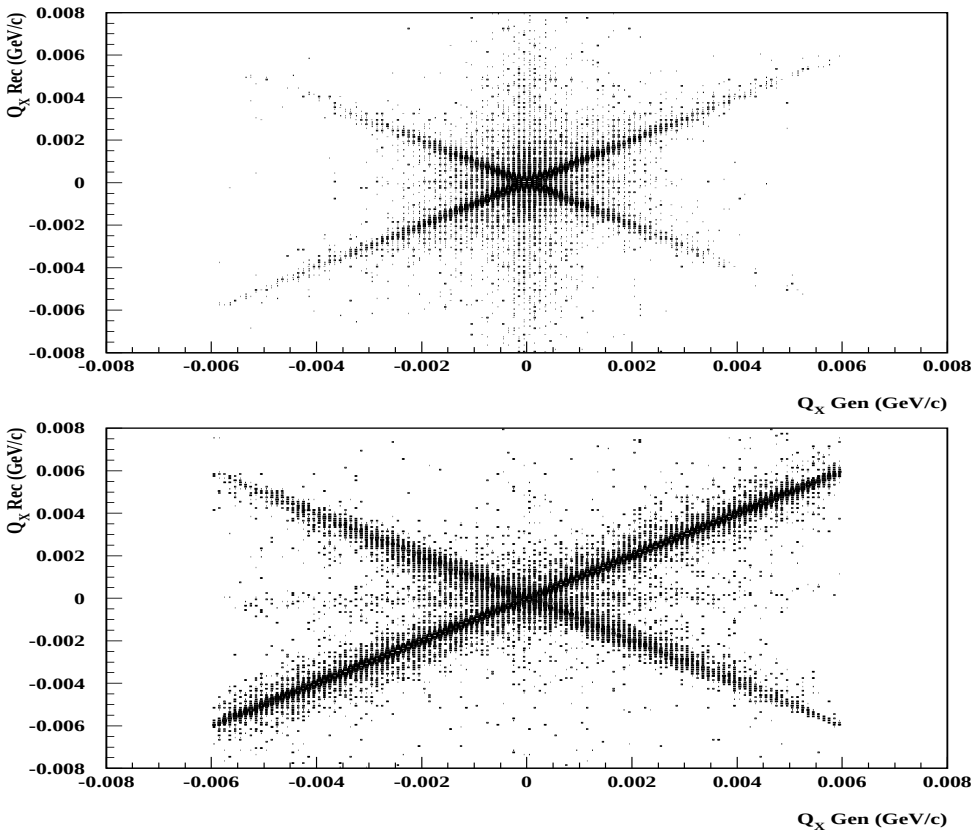

Fig. 7. *Correlation between generated and reconstructed Q_X for atoms pairs (top) and Coulomb pairs (bottom).*

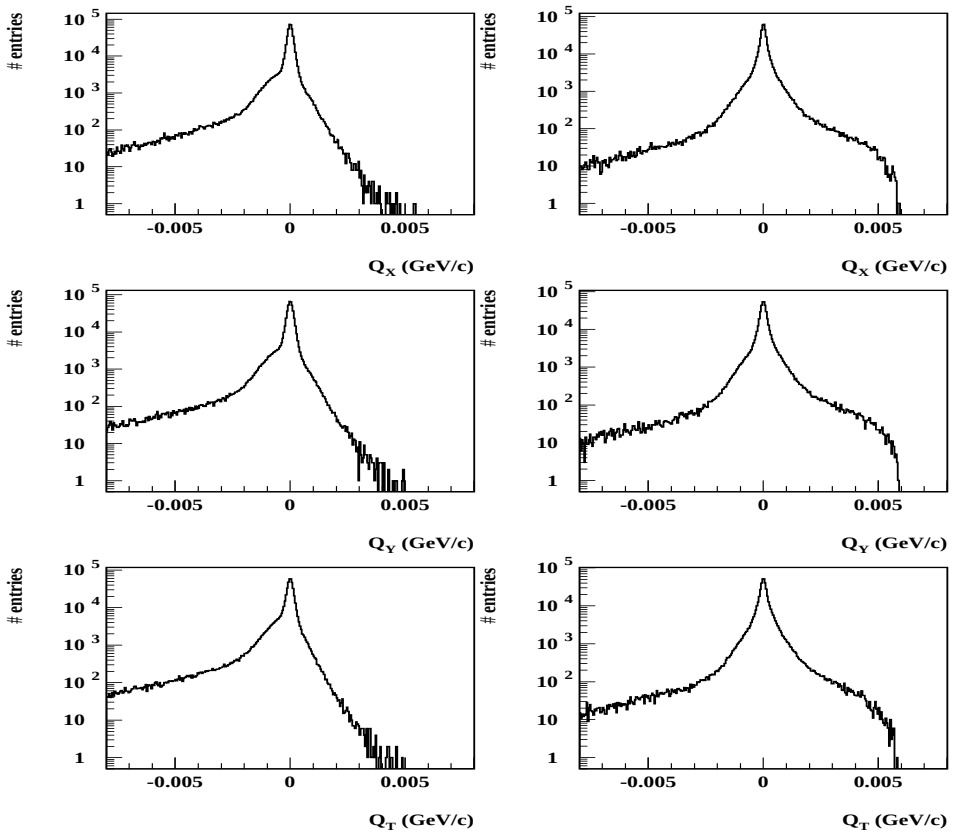

Fig. 8. *Resolution defined as* $|Q_i^{gen}| - |Q_i^{rec}|$ *for* $|Q_X|$ *(top) ,* $|Q_Y|$ *(center) and* Q_T *(bottom). Atoms pairs are shown at the left, and Coulomb pairs at the right hand side.*

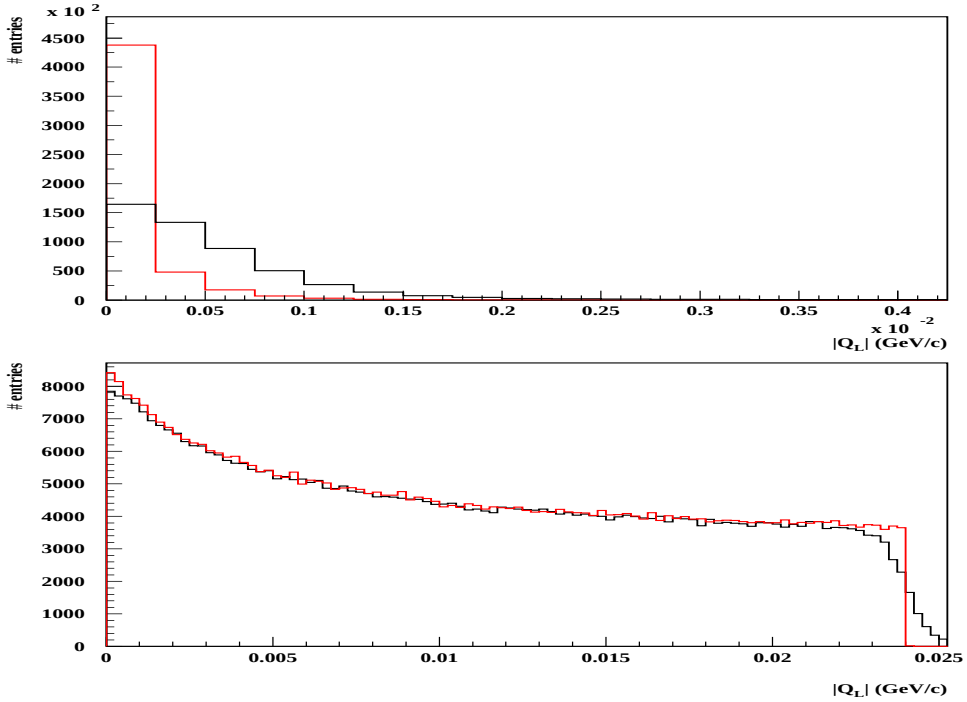

Fig. 9. *Comparison between generated $|Q_L|$ spectrum G_1 (red), and reconstructed spectrum R_1 (black) for atom pairs (top), and for Coulomb pairs (bottom).*

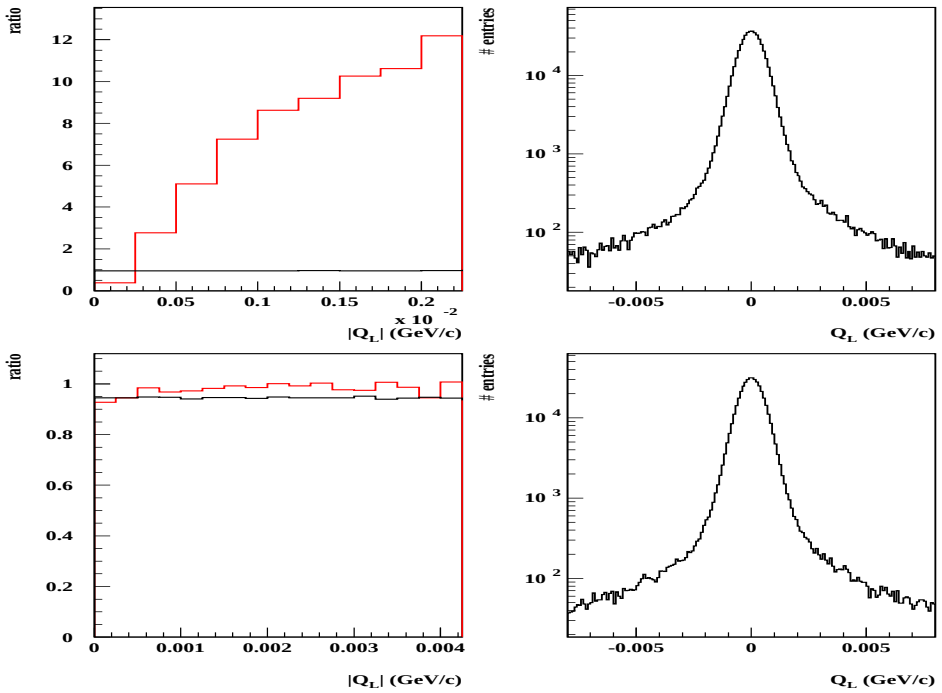

Fig. 10. *Ratios G_1/G_0 (black) and R_1/G_1 (red) for the lines shown in figure 9 for $|Q_L|$ of atom pairs (top left). and for Coulomb pairs (bottom left). Resolution plots for Q_L are also shown at the right hand side.*

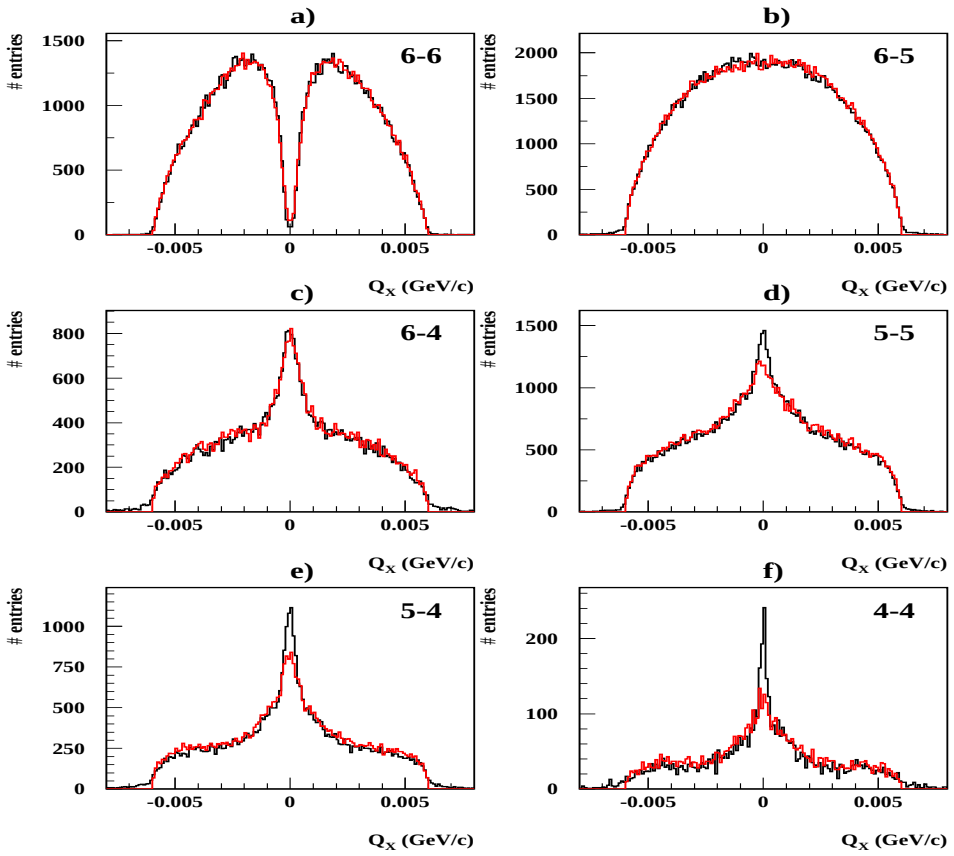

Fig. 11. *Q_X spectrum of the reconstructed Coulomb pairs shown in figure 1 (bottom) separated into 6 categories according to the number of hits in each track, namely : 6-6 , 6-5 , 6-4 , 5-5 , 5-4 , 4-4.*

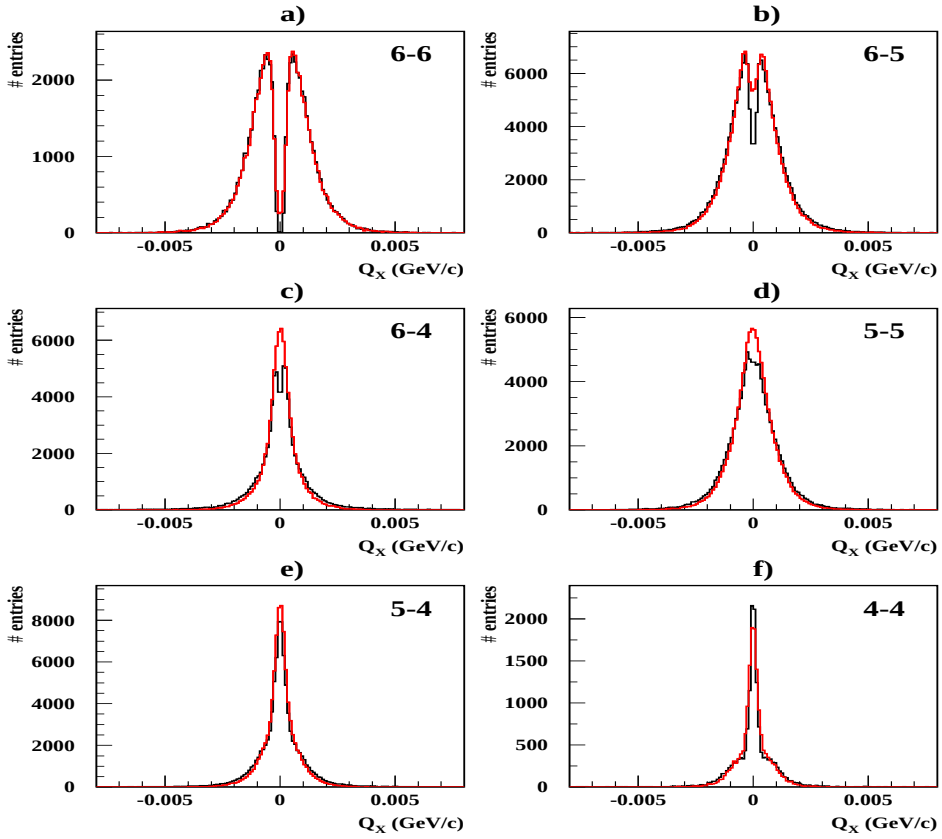

Fig. 12. *Q_X spectrum of reconstructed atom pairs shown in figure 1 (top) , separated into 6 categories according to the number of hits in each track, namely : 6-6, 6-5 , 6-4 , 5-5 , 5-4 , and 4-4.*

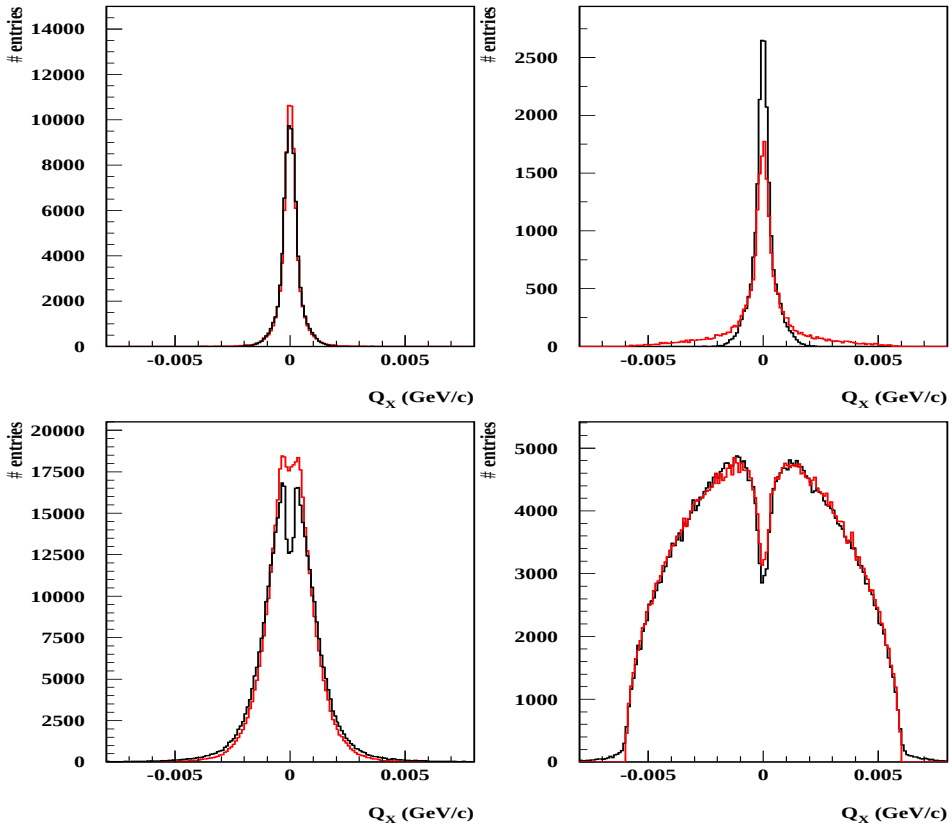

Fig. 13. *Reconstructed Q_X (black) along with generated G_1 spectrum (red) for events with a single SFD hit shared by both tracks (top), and for the remainder (bottom). Left hand side for atom pairs, right for Coulomb pairs.*

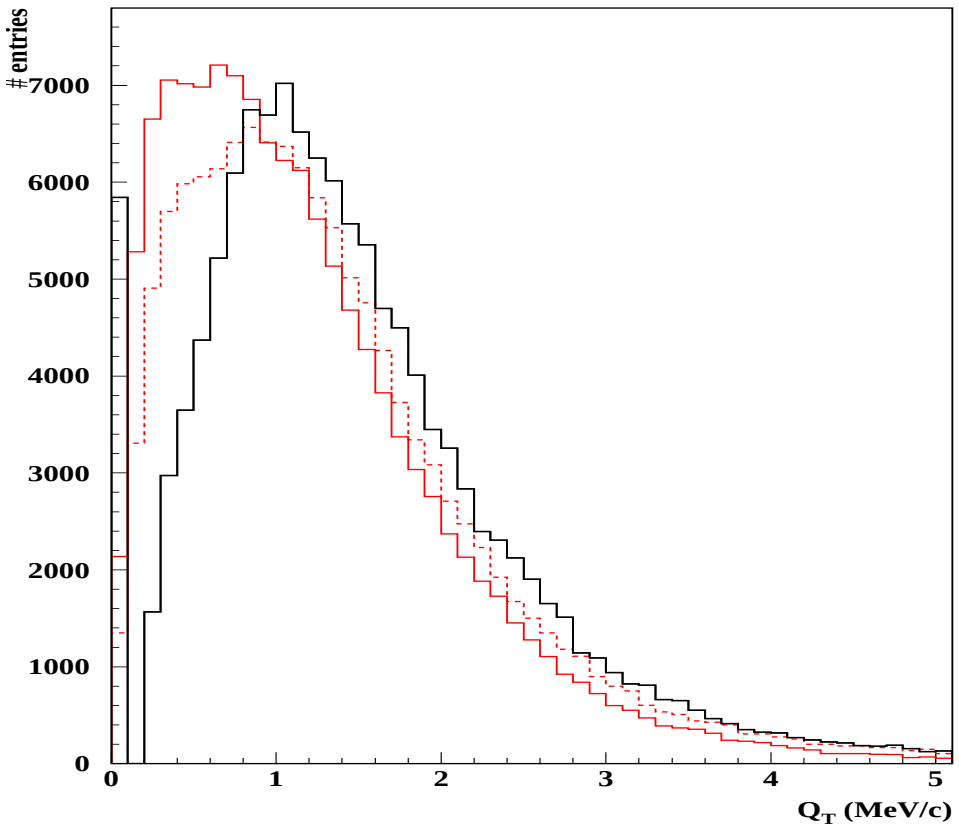

Fig. 14. *Reconstructed Q_T spectrum for atom pairs when only SFD hits are used in the final vertex fit (black). Full-tracking reconstruction is shown as dotted red line, and the true spectrum (G_1) is shown as a red line. The spike at zero corresponds to identical SFD hits.*

4 Conclusions

The results presented in this addendum confirm the conclusions established earlier in note [1], namely that the full-tracking reconstruction is efficient and well-behaved for both pionium signal and Coulomb pairs. The consequences of the improvements reported here can be summarized as follows:

- The two-track inefficiency for wide-angle pairs has been significantly reduced, thus making the spurious enhancement at very low Q_X and Q_Y nearly disappear. This provides a smoother and more accurate reconstruction for Coulomb pairs.
- Pionium signal reconstruction has become, on the other hand, less prompt, due to a corresponding increase of the effect of detector backgrounds. Atom loss related to the tracking at the standard $Q_T < 4\ MeV/c$ cut is however small (2.65%), and even smaller at $Q_T < 5\ MeV/c$ (1.80%).
- The overall acceptance for pionium pairs and for Coulomb pairs have both increased, and are now equal to each other as function of Q_T, as shown by G_1/G_0 line in figure 6.

References

[1] DIRAC note 05-15: Full-Tracking Resolution in DIRAC with 2001 Data , B. Adeva, A. Romero and O. Vázquez Doce.

[2] DIRAC note 05-11: Study of SFD Efficiency using MSGC Detector for 2001 Data , B. Adeva, A. Romero and O. Vázquez Doce.